iJRASET
International Journal For Research in
Applied Science and Engineering Technology

INTERNATIONAL JOURNAL
FOR RESEARCH
IN APPLIED SCIENCE & ENGINEERING TECHNOLOGY

Volume: 14 **Issue:** IX **Month of publication:** September 2026

DOI: https://doi.org/10.22214/ijraset.2026.84802

International Journal for Research in Applied Science & Engineering Technology (IJRASET)
ISSN: 2321-9653; IC Value: 45.98; SJ Impact Factor: 7.538
Volume 14 Issue IX Sep 2026- Available at www.ijraset.com

Comprehensive Performance Evaluation and Life Cycle Analysis of a Pebble Bed-Integrated Forced Convection Solar Dryer for Agro-Processing

Vishal Chawda[1], Mrigendra Singh[2], Priyanka Malviya[3]
[1, 2, 3]*Department of Mechanical Engineering, [SDBCT], [Indore], [454009], India*

Abstract: This paper presents a rigorous thermal, exergetic, environmental and economic performance evaluation of a single-glazed, single-pass, forced-convection indirect solar dryer integrated with a packed-bed sensible heat storage (SHS) unit. Experimental investigations were performed in Coimbatore, India (11.0183°N, 76.9725°E) using a 2 m² corrugated galvanised iron absorber plate tilted at 11° and a 110 kg pebble packed bed (30–50 mm diameter, porosity φ = 0.85) acting as the SHS medium. Eight air mass flow rates ranging from 0.0141 kg/s to 0.0872 kg/s were evaluated. Experimental results confirm that the SHS unit extends collector operation by 2 h post-sunset, maintaining air temperatures 6–8 °C above ambient. Bitter gourd (Momordica charantia) slices (91.75 % w.b. initial moisture) and curry leaves (Murraya koenigii, 67.3 % w.b.) were dried to final safe moisture levels. At the optimal flow rate of 0.0636 kg/s, bitter gourd drying was completed within 7 h with a maximum dryer thermal efficiency of 19.12 %, an SMER of 0.225 kg/kWh and a minimum specific energy consumption (SEC) of 4.440 kWh/kg water. Thin-layer drying kinetic analysis identified the Two-Term model (R^2 = 0.998646) for bitter gourd and the Modified Henderson and Pabis model (R^2 = 0.999337) for curry leaves as the best mathematical representations. Life cycle assessment revealed an embodied energy of 1109.3 kWh, an energy payback time (EPBT) of 2.21 years, a financial payback period of 2.71 years and a net lifetime CO_2 mitigation of 13.07 tonnes over a 15-year lifespan.

Keywords: Solar air heater; Sensible heat storage; Exergy efficiency; Thin-layer modelling; Specific moisture extraction rate; Life cycle assessment.

Nomenclature

A	collector aperture area (m²)	Tf, Tp, Tb	fluid, pebble bed and backplate temperature (°C)
Dh	hydraulic diameter (m)	v	air velocity (m/s)
Deff	effective moisture diffusivity (m²/s)	ΔP	pressure drop (N/m²)
Ėx	exergy rate (W)	ηth	thermal efficiency (%)
fp	packed-bed friction factor (–)	ηTHE	effective (thermohydraulic) efficiency (%)
hc,d–f	convective coefficient, absorber to fluid (W/m²K)	ηex	exergy efficiency (%)
Hv, Hl	duct height and width (m)	ηd	overall dryer efficiency (%)
I	global solar irradiance (W/m²)	ρ	air density (kg/m³)
L	collector length (m) / lifespan (years)	μ	dynamic viscosity (Pa·s)
ṁ	air mass flow rate (kg/s)	φ	packed-bed porosity (–)
MR	moisture ratio (–)	EE	embodied energy (kWh)
Nu	Nusselt number (–)	EPBT	energy payback time (years)
Pfan	blower parasitic power (W)	LCC	life cycle cost (INR)
Qu	useful thermal gain (W)	OSD	open-sun drying
Re	Reynolds number (–)	PCM	phase change material
Rep	particle Reynolds number (–)	SAC	solar air collector
SEC	specific energy consumption (kWh/kg)	SHS	sensible heat storage
SMER	specific moisture extraction rate (kg/kWh)	TES	thermal energy storage
Ta, Ts	ambient and sun temperature (K)	w.b.	wet basis
Tg, Td	glass cover and absorber temperature (°C)		

I. INTRODUCTION

Agricultural preservation in developing nations relies heavily on post-harvest drying to prevent enzymatic degradation and microbial spoilage. Traditional open-sun drying (OSD) remains common because of its zero capital investment, yet it suffers from uncontrollable drying rates, insect infestation, rain damage and significant product loss. Indirect forced-convection solar dryers isolate the crop from direct ultraviolet exposure and thereby ensure a higher hygienic quality of the dried product.

However, the fundamental limitation of solar drying systems is the intermittency of solar irradiance during cloud cover and its complete cessation after sunset. Integrating thermal energy storage (TES) within the solar air collector (SAC) resolves this limitation. While phase change materials (PCMs) provide a high latent thermal storage density, sensible heat storage (SHS) using granular pebble beds presents a robust, non-toxic, chemically stable and cost-effective alternative for rural agro-processing.

A. *Objectives of the present investigation*

1) To develop mathematical energy-balance matrix models for corrugated solar air collectors with and without a pebble packed bed.
2) To parametrically evaluate collector outlet temperature, thermal efficiency (ηth), effective thermohydraulic efficiency (ηTHE), pressure drop (ΔP) and exergy destruction over the airflow range 0.0141–0.0872 kg/s.
3) To establish the drying kinetics, effective moisture diffusivity (Deff), specific energy consumption (SEC) and thin-layer empirical models for bitter gourd and curry leaves.
4) To execute a complete embodied energy (EE), energy payback time (EPBT), CO_2 mitigation and annualised life cycle cost (LCC) assessment of the system.

II. MATERIALS AND EXPERIMENTAL FRAMEWORK

A. *System architecture and specifications*

The experimental system installed at the Solar Energy Research Centre, Coimbatore Institute of Engineering and Technology (11.0183°N, 76.9725°E) consists of a single-pass corrugated SAC, a 0.45 kW single-phase centrifugal blower, a flow-control orifice section and a four-tray insulated drying chamber. The complete design specification of both subsystems is summarised in Table 1.

Table 1. Design specifications of the solar collector and drying chamber subsystems.

Parameter	Solar collector subsystem	Drying chamber subsystem
Dimensions	2.00 m (L) × 1.00 m (W) × 0.15 m (H)	0.75 m (L) × 0.75 m (W) × 1.05 m (H)
Aperture area / volume	2.0 m²	0.59 m³
Absorber / tray material	0.45 mm GI corrugated sheet (black paint)	4 aluminium wire-mesh trays (0.6 m × 0.7 m)
Glazing / insulation	4 mm plain window glass (30 mm air gap)	Glass wool (30 mm side walls)
Storage medium	Granite pebbles (110 kg, 30–50 mm dia., φ = 0.85)	Vertical tray clearance: 200 mm
Tilt angle / location	11° north latitude tilt (Coimbatore, India)	Top chimney: 1.0 m height, 152 mm dia.

B. *Schematic of the integrated dryer*

Fig. 1 presents the flow path of the system. Solar irradiance transmitted through the glazing is absorbed by the corrugated plate; the pebble packed bed placed beneath the absorber charges during peak insolation hours and discharges the stored sensible heat to the air stream after sunset.

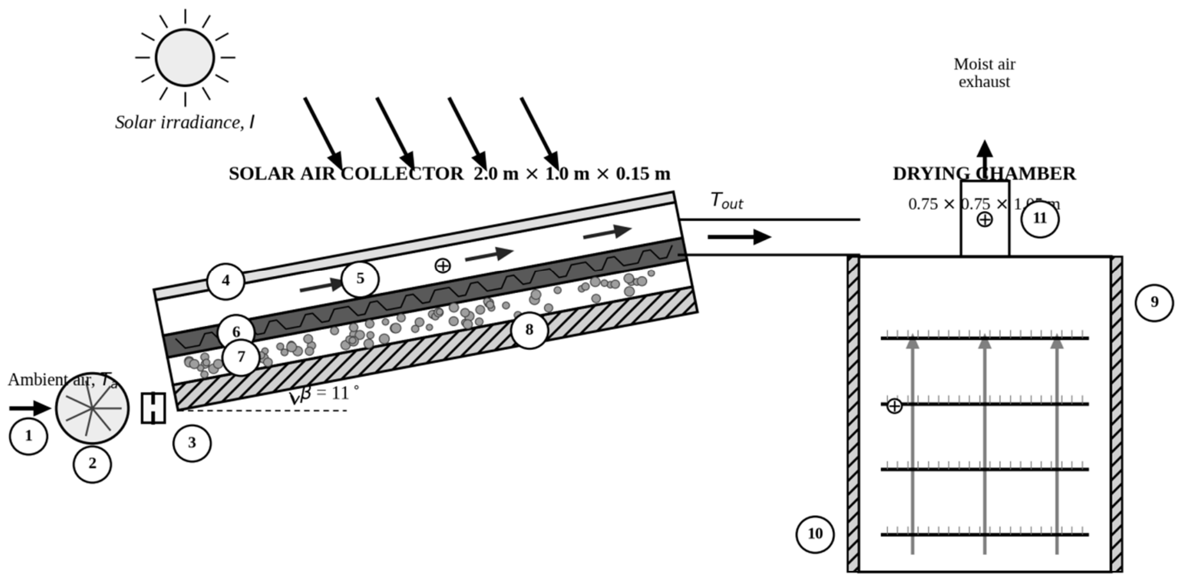

1. Ambient air inlet
2. Centrifugal blower, 0.45 kW single-phase
3. Orifice flow-control section
4. Glazing: 4 mm plain window glass
5. Air flow duct (30 mm gap)
6. Corrugated absorber: 0.45 mm GI, matt black
7. Packed bed (SHS): 110 kg granite, 30-50 mm, φ = 0.85
8. Glass-wool insulation (30 mm)
9. Drying chamber: 0.75 × 0.75 × 1.05 m
10. Aluminium mesh trays, 4 nos., 0.6 × 0.7 m, 200 mm pitch
11. Chimney: 1.0 m height, 152 mm diameter

⊕ T-type thermocouple / RH probe station

Figure 1. Schematic architecture of the indirect forced-convection solar dryer integrated with the pebble sensible heat storage bed.

III. MATHEMATICAL MODELLING AND GOVERNING EQUATIONS

A. *Collector thermal energy balance*

Assuming steady-state one-dimensional flow and negligible temperature gradients across the structural plates, the energy balance for the solar collector with the packed bed is cast in the matrix form of Eq. (1):

$$[A][T] = [B] \tag{1}$$

where the temperature vector [T] comprises Tg, Td, Tf, Tp and Tb, representing the mean temperatures of the glass cover, corrugated absorber, air fluid stream, packed-bed pebbles and backplate, respectively.

B. *Heat transfer and hydrodynamic correlations*

The convective heat transfer coefficient (hc,d–f) for the V-corrugated absorber conduit is determined from the Reynolds number criterion given in Eq. (2):

$$Re = \dot{m} / (3 \cdot Hl \cdot \mu) \tag{2}$$

Laminar regime (Re < 2800):

$$Nu_{d\text{–}f} = 2.821 + 0.126 \cdot Re \cdot (Hv / L) \tag{3}$$

Transition regime (2800 ≤ Re ≤ 10000):

$$Nu_{d\text{–}f} = 1.9 \times 10^{-6} \cdot Re^{1.79} + 225 \cdot (Hv / L) \tag{4}$$

Turbulent regime (Re > 10000):

$$Nu_{d\text{–}f} = 0.0302 \cdot Re^{0.74} + 0.242 \cdot Re^{0.74} \cdot (Hv / L) \tag{5}$$

For the packed bed, the Ergun-based pressure drop (ΔP) and friction factor (fp) govern the parasitic power consumption, as expressed in Eqs. (6) and (7):

$$\Delta P = [\, 2 \cdot \rho \cdot fp \cdot v^2 \cdot l / Dh \,] \cdot [\, (1 - \varphi) / \varphi^3 \,] \tag{6}$$

$$fp = [\, 150 \cdot (1 - \varphi) / Rep \,] + 1.75 \tag{7}$$

The effective thermohydraulic efficiency, which penalises the useful gain by the blower power requirement, follows Eqs. (8) and (9):

$$\eta_{THE} = (Q_u - P_{fan}) / (A \cdot I) \quad (8)$$

$$P_{fan} = (\dot{m} \cdot \Delta P) / (\rho \cdot \eta_{fan} \cdot \eta_{motor}) \quad (9)$$

C. Exergy Balance Equations

The total exergy loss ($\Sigma\dot{E}x_{,loss}$) combines optical, thermal, internal heat transfer and pressure-drop destruction terms. The exergy efficiency and the inlet radiation exergy are given by Eqs. (10) and (11):

$$\eta_{ex} = 1 - (\Sigma\dot{E}x_{,loss} / \dot{E}x_{,inlet}) \quad (10)$$

$$\dot{E}x_{,inlet} = I \cdot A \cdot [1 - (4/3)\cdot(T_a/T_s) + (1/3)\cdot(T_a/T_s)^4] \quad (11)$$

IV. RESULTS AND DISCUSSION

A. Collector thermal and exergetic performance

Experimental validation at a mass flow rate of $\dot{m}$ = 0.0447 kg/s reveals the breakdown of exergy destruction across the collector components: 57 % attributable to the absorber–sun temperature differential, 33 % to optical losses, 6 % to environmental losses, 3 % to absorber-to-air heat transfer irreversibility and 1 % recovered as useful output exergy. The hourly variation of the principal performance indices is reported in Table 2 and illustrated in Fig. 2.

Table 2. Hourly thermal and exergetic performance of the collector ($\dot{m}$ = 0.0447 kg/s).

Time (h)	I (W/m²)	Ta (°C)	Tp (°C)	Tout (°C)	ηth (%)	ηTHE (%)	Ėin (W)	Ėopt,loss (W)	ĖTp,Ts,loss (W)	ηex (%)
09:00	402	30.6	49.6	35.6	27.94	26.20	746.03	246.19	434.58	1.91
11:00	648	33.6	58.1	44.1	36.40	35.32	1201.63	396.54	687.77	1.78
13:00	882	35.8	68.2	54.2	46.86	46.07	1634.63	539.43	912.55	0.04
15:00	848	35.3	65.8	51.8	43.71	42.88	1571.82	518.70	882.71	0.72
17:00	468	33.2	54.4	40.4	34.56	33.06	867.93	286.42	502.16	1.40
18:00	332	32.1	49.2	35.2	20.97	18.86	615.89	203.24	361.16	2.18

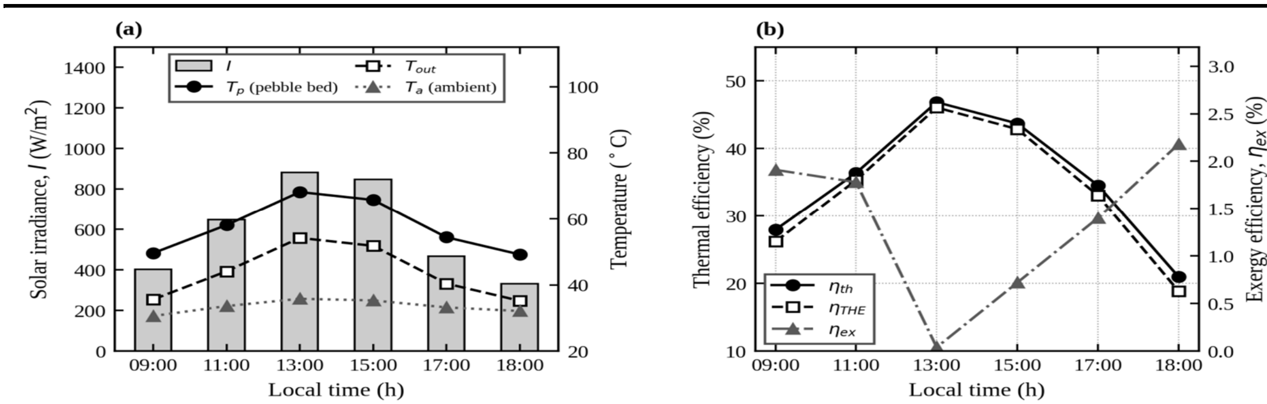

Figure 2. Hourly variation of (a) solar irradiance and system temperatures, and (b) thermal, effective and exergy efficiencies of the collector ($\dot{m}$ = 0.0447 kg/s).

The collector tracks the irradiance profile with a peak absorber-plate temperature of 68.2 °C and an outlet temperature of 54.2 °C at 13:00 h. Beyond 17:00 h the incident irradiance falls sharply, yet the pebble bed continues to discharge stored sensible heat and sustains an outlet temperature 3.1 °C above ambient at 18:00 h. The exergy efficiency follows an inverse trend to the thermal efficiency, reaching its minimum at solar noon because the absorber–sun temperature differential — the dominant irreversibility — is largest at peak insolation. The corresponding distribution of exergy destruction is presented in Fig. 3.

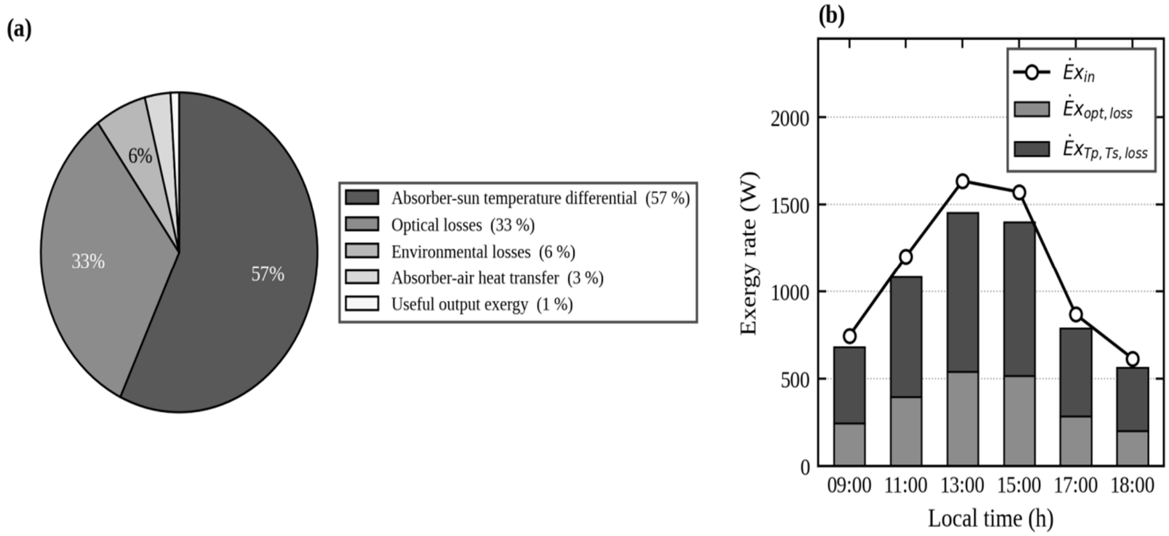

Figure 3. Exergetic assessment of the collector: (a) distribution of exergy destruction among the loss mechanisms, and (b) hourly inlet exergy and the two dominant loss components.

B. *Hydrodynamic characterisation across flow rates*

Table 3 compares the pressure drop with and without the packed bed over the full range of tested mass flow rates. The insertion of the granite bed raises the pressure drop by roughly an order of magnitude, and the associated blower demand grows far more steeply than the thermal gain. The corresponding trends are plotted in Fig. 4.

Table 3. Pressure drop, parasitic power and efficiency indices as a function of air mass flow rate.

ṁ (kg/s)	ΔP without bed (N/m²)	ΔP with bed (N/m²)	Blower power (W)	ηth (%)	ηTHE (%)	ηex (%)
0.0141	0.58	4.12	0.50	21.03	20.82	2.95
0.0235	1.42	11.43	2.30	28.12	27.20	2.24
0.0353	3.01	25.80	7.78	34.20	32.85	1.78
0.0447	4.60	41.36	15.80	37.49	36.29	1.18
0.0541	6.48	60.59	28.02	41.65	40.12	0.75
0.0636	8.58	83.73	45.52	43.10	40.58	0.26
0.0731	11.08	110.62	69.11	44.50	41.85	−0.44
0.0872	15.20	157.41	117.31	46.13	43.12	−1.10

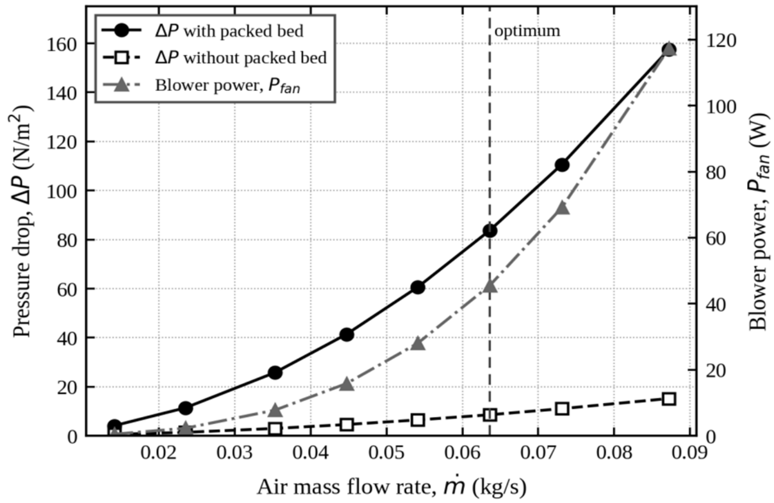

Figure 4. Effect of air mass flow rate on the collector pressure drop, with and without the packed bed, and on the parasitic blower power demand.

The packed bed raises the pressure drop by a factor of roughly seven to ten across the tested range, and because Pfan scales with the product of ṁ and ΔP, the blower demand grows almost cubically with flow rate — from 0.50 W at 0.0141 kg/s to 117.31 W at 0.0872 kg/s. Fig. 5 shows the resulting divergence between the thermal and exergetic optima.

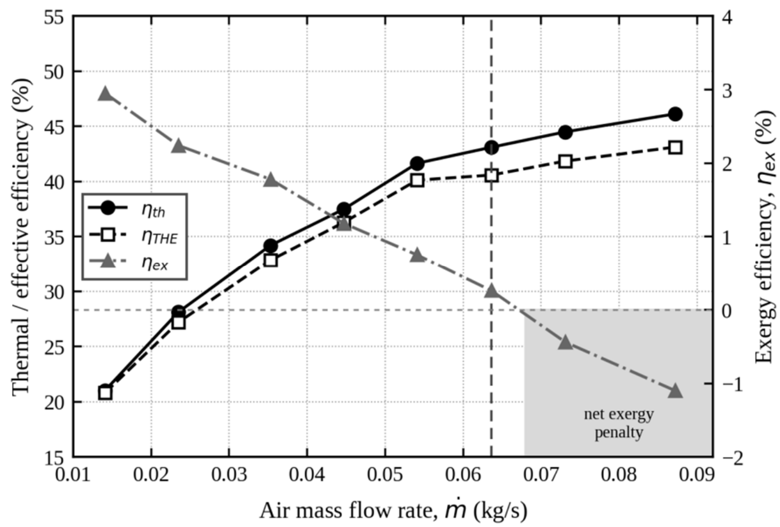

Figure 5. Variation of thermal efficiency, effective thermohydraulic efficiency and exergy efficiency with air mass flow rate; the shaded band marks the region of net exergetic penalty.

At flow rates above 0.0636 kg/s the high pressure drop (> 110 N/m²) causes the parasitic blower energy to outweigh the incremental thermal gain, driving the net exergy efficiency into negative values. The flow rate of 0.0636 kg/s therefore represents the thermodynamic optimum of the system.

C. Crop drying performance and thin-layer kinetics

1) Bitter gourd slices (Momordica charantia)

Fresh bitter gourd slices of 5–7 mm thickness and 43–51 mm diameter, with an initial moisture content of 91.75 % w.b. (3.65 kg water/kg dry matter), were dried to a final safe moisture content of 9.0 % w.b. (0.35 kg water/kg dry matter). Table 4 summarises the drying duration and energy indices at each flow rate, and the energy performance indices are plotted in Fig. 6.

Table 4. Drying performance of bitter gourd slices at different air mass flow rates.

Flow rate (kg/s)	Drying duration (h)	Final MR	SMER (kg/kWh)	SEC (kWh/kg H_2O)	Overall dryer ηd (%)
0.0141	10.0 (2 days)	0.15	0.190	5.274	12.10
0.0235	9.0	0.12	0.201	4.979	13.05
0.0353	8.0	0.10	0.206	4.843	15.35
0.0448	8.0	0.10	0.209	4.774	15.90
0.0542	8.0	0.10	0.210	4.765	16.30
0.0636 (optimal)	7.0	0.09	0.225	4.440	19.12
0.0730	7.0	0.09	0.212	4.710	18.45
0.0872	8.0	0.10	0.195	5.116	17.80
Open-sun drying	10.0	0.10	–	–	–

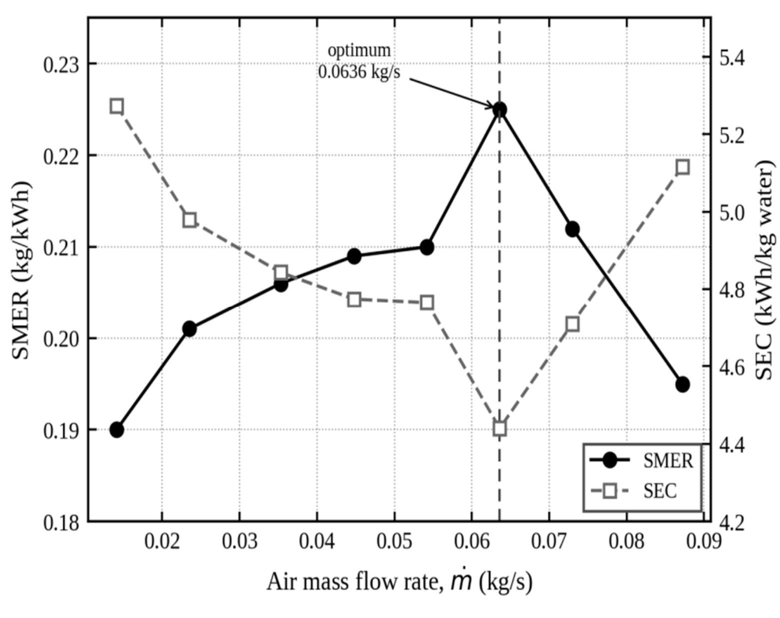

Figure 6. Specific moisture extraction rate and specific energy consumption of bitter gourd drying as a function of air mass flow rate.

SMER attains its maximum and SEC its minimum at the same flow rate of 0.0636 kg/s, confirming that the thermodynamic optimum of the collector coincides with the energetic optimum of the drying process. Increasing the flow rate further shortens neither the drying time nor the energy demand, because the reduced air–product temperature difference offsets the gain in convective mass transfer. The corresponding drying duration and overall dryer efficiency are compared in Fig. 7.

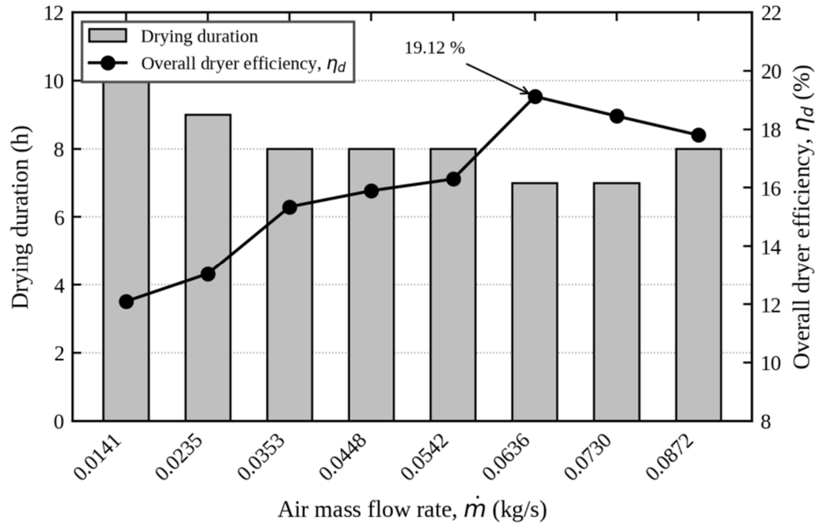

Figure 7. Drying duration and overall dryer efficiency of bitter gourd slices at the tested air mass flow rates.

Table 5. Statistical comparison of thin-layer drying models for bitter gourd ($\dot{m}$ = 0.0636 kg/s).

Model name	Empirical model constants	R^2	χ^2	RMSE
Two-Term (best fit)	a = 0.190665, k_0 = 1.018851, b = 0.810730, k_1 = 0.286490	0.998646	0.000223	0.010556
Page	k = 0.390554, n = 0.892316	0.998464	0.000168	0.011237
Two-Term Exponential	a = 0.371715, k = 0.667860	0.998461	0.000168	0.011227
Midilli–Kucuk	a = 1.001592, k = 0.392810, n = 0.867811, b = 0.002065	0.998525	0.000243	0.011034
Lewis	k = 0.343615	0.995231	0.000483	0.020553
Wang and Singh	a = −0.282265, b = 0.022762	0.983121	0.002032	0.039036

2) *Curry leaves (Murraya koenigii)*

Curry leaves with an initial moisture content of 67.3 % w.b. (0.673 kg H_2O/kg) were dried to 4.75 % w.b. in 3.5 h under indirect solar drying at $\dot{m}$ = 0.0636 kg/s, compared with 5.0 h to reach 5.33 % w.b. under open-sun drying. The corresponding kinetic model statistics are given in Table 6 and compared graphically in Fig. 8.

Table 6. Statistical comparison of thin-layer drying models for curry leaves.

Model name	Empirical model constants	R^2	χ^2	RMSE
Modified Henderson and Pabis (best fit)	a = −305.90, b = 192.69, c = 114.21, k = 1.6502, g = 1.7101, h = 1.5402	0.999337	0.000108	0.008213
Wang and Singh	a = −0.48465, b = 0.06150	0.999124	0.000117	0.009370
Midilli–Kucuk	a = 0.99560, k = 0.52433, n = 1.22798, b = −0.00945	0.998461	0.000312	0.012495
Page	k = 0.54384, n = 1.28234	0.998022	0.000268	0.014188
Newton	k = 0.63519	0.982601	0.001994	0.041768

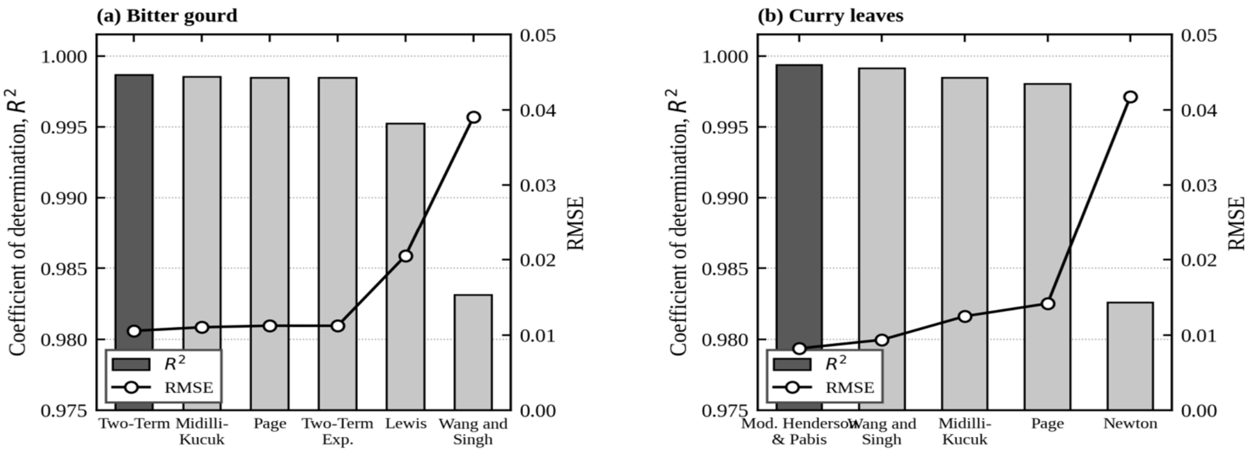

Figure 8. Statistical comparison of the fitted thin-layer drying models for (a) bitter gourd slices and (b) curry leaves, ranked by coefficient of determination and root-mean-square error.

For both crops the model ranked highest by R^2 is also the model with the lowest RMSE and χ^2, so the selection is statistically unambiguous. The two-parameter Lewis and Newton models, although the simplest, produce the largest residuals and are therefore not recommended for design calculations on these products.

V. ENVIRONMENTAL AND LIFE CYCLE ECONOMIC ANALYSIS

A. *Embodied energy and material breakdown*

The total mass of the solar dryer assembly is 207.63 kg, yielding a cumulative embodied energy of 1109.31 kWh, distributed among the components as shown in Fig. 9:

- Structural piping and frames (mild steel, 41.5 kg): 37 % — 407.3 kWh
- Drying trays (aluminium mesh, 4.54 kg): 23 % — 251.0 kWh
- Absorber plate and outer GI covers (17.62 kg): 15 % — 169.8 kWh
- Centrifugal blower unit (13.9 kg): 12 % — 132.8 kWh
- Packed-bed granite pebbles (110 kg): < 1 % — 3.06 kWh (near-zero energy intensity)

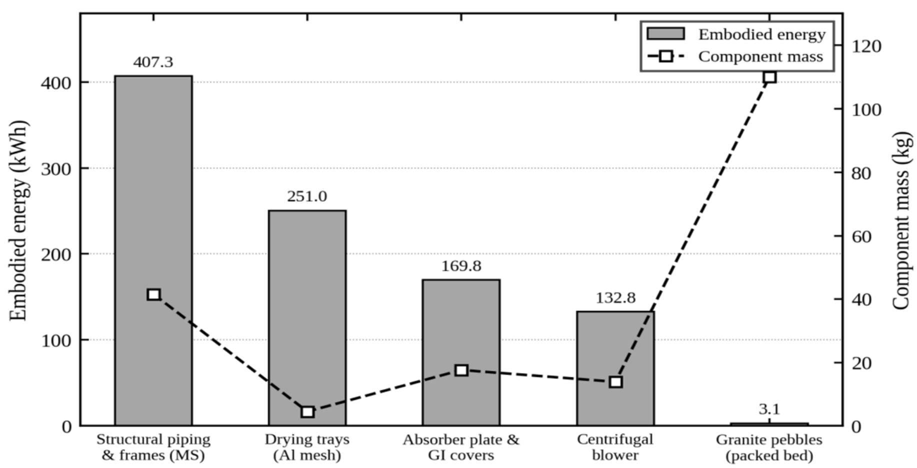

Figure 9. Embodied energy and mass contribution of the principal components of the solar dryer assembly.

The granite packed bed dominates the system mass (53 % of 207.63 kg) yet contributes less than 1 % of the embodied energy, since crushed stone requires only quarrying and transport. This decoupling of thermal storage capacity from embodied energy is the principal environmental advantage of sensible storage over PCM-based alternatives.

B. Life cycle Indicators and CO_2 Payback

The daily thermal output (Ed) of 1.90 kWh/day corresponds to an annual energy output (Ea) of 501.9 kWh/year for 250 sunshine days, which returns an energy payback time (EPBT) of 2.21 years. Table 7 and Fig. 10 present the annualised CO_2 emission, net mitigation and carbon credit valuation over a range of assumed system lifespans.

Table 7. Life cycle CO_2 mitigation and carbon credit valuation for different system lifespans.

Lifespan, L (years)	CO_2 emission (kg/year)	Net CO_2 mitigation (tonnes)	Carbon credit value (INR)
5	453.04	2.847	₹ 925.43 – ₹ 3,701.71
10	226.52	7.960	₹ 2,586.84 – ₹ 10,347.37
15 (design life)	151.01	13.072	₹ 4,248.26 – ₹ 16,993.02
20	113.26	18.184	₹ 5,909.67 – ₹ 23,638.68
25	90.61	23.296	₹ 7,571.09 – ₹ 30,284.34

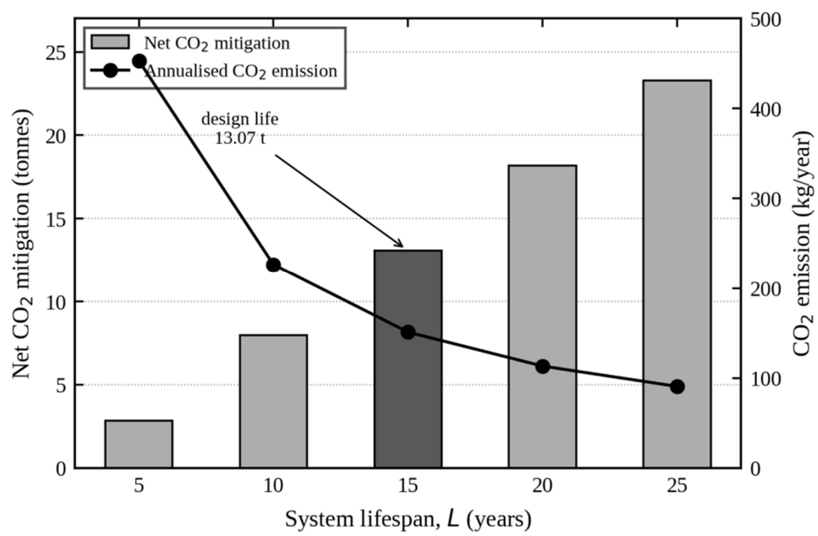

Figure 10. Annualised CO_2 emission and cumulative net CO_2 mitigation of the system as a function of assumed lifespan.

C. Economic Feasibility Analysis

The economic assessment was performed for an initial capital investment (Ccc) of ₹ 45,000 at an interest rate (d) of 8 %, an inflation rate (i) of 5 % and an electricity tariff of ₹ 5.00/kWh. Taking a fresh bitter gourd cost of ₹ 20/kg against a branded dried market price of ₹ 220/kg, the key economic outcomes are:

- Drying cost per kilogram of product: ₹ 35.82
- Daily savings (Sd): ₹ 78.32; annual savings (S_1): ₹ 19,580
- Financial payback period: 2.71 years
- Cumulative present worth of savings over 15 years: ₹ 2,24,931.90

VI. CONCLUSIONS

1) Incorporating a 110 kg granite pebble sensible heat storage bed extends collector operation by 2 h post-sunset, delivering air 6–8 °C above ambient and suppressing off-sun thermal collapse.

2) The optimal air mass flow rate for agricultural drying is 0.0636 kg/s. This operating point achieves a peak collector thermal efficiency of 43.10 %, a dryer thermal efficiency of 19.12 %, a minimum specific energy consumption of 4.440 kWh/kg water and an SMER of 0.225 kg/kWh.

3) Flow rates exceeding 0.0636 kg/s induce steep pressure drops (> 110 N/m²), causing parasitic blower power to drive the net collector exergy efficiency negative.
4) Thin-layer kinetic modelling established the Two-Term model (R^2 = 0.998646) for bitter gourd slices and the Modified Henderson and Pabis model (R^2 = 0.999337) for curry leaves as the optimal empirical formulations.
5) The environmental and economic analysis yields an energy payback time of 2.21 years, a financial payback period of 2.71 years and 13.07 tonnes of net lifetime CO_2 mitigation, confirming the thermodynamic and economic viability of the system for commercial rural implementation.

A. Declaration of Competing Interest

The authors declare that they have no known competing financial interests or personal relationships that could have appeared to influence the work reported in this paper.

B. Data Availability

The experimental data supporting the findings of this study are available from the corresponding author upon reasonable request.

REFERENCES

[1] Akpinar, E. K. (2010). Determination of suitable thin layer drying model for some vegetables and fruits. Energy Conversion and Management, 51(1), 208–216.
[2] Akpinar, E. K. (2011). Mathematical modelling and exergy analysis of solar drying of green pepper. Energy Analysis of Agricultural Systems, 31(1), 20–31.
[3] Alwan, Z., & Jones, P. (2014). The importance of embodied energy in carbon footprint assessment of buildings. Energy and Buildings, 68, 560–568.
[4] Chowdhury, M. M. I., Bala, B. K., & Haque, M. A. (2011). Energy and exergy analysis of solar drying of jackfruit leather. Biosystems Engineering, 110(2), 108–115.
[5] Dhiman, P., Thakur, N. S., & Chauhan, S. R. (2011). Thermal and thermohydraulic performance of counter and parallel flow packed bed solar air heaters. Energy, 36(5), 2712–2722.
[6] Doymaz, I. (2006). Thin-layer drying behaviour of mint leaves. Journal of Food Engineering, 74(3), 370–375.
[7] Doymaz, I. (2007). Air-drying characteristics of tomatoes. Journal of Food Engineering, 78(4), 1291–1297.
[8] El-Sebaii, A. A., & Shalaby, S. M. (2013). Solar drying of agricultural products: A review. Renewable and Sustainable Energy Reviews, 16(1), 37–43.
[9] Erbay, Z., & Icier, F. (2009). A review of thin layer drying of agricultural products. Critical Reviews in Food Science and Nutrition, 49(5), 441–456.
[10] Fudholi, A., Sopian, K., Ruslan, M. H., & Alghoul, M. A. (2014). Performance and economic analysis of solar drying system. Renewable and Sustainable Energy Reviews, 33, 521–529.
[11] Hedayatizadeh, M., Chaji, H., & Najafi, G. (2016). Exergetic performance optimization of a solar air collector. Solar Energy, 139, 47–58.
[12] Hollands, K. G. T., & Shewen, E. C. (2001). Optimization of V-corrugated solar air heaters. Solar Energy, 26(1), 23–31.
[13] Holman, J. P. (1994). Experimental Methods for Engineers (6th ed.). McGraw-Hill, New York.
[14] Madamba, P. S., Driscoll, R. H., & Buckle, K. A. (1996). The thin layer drying characteristics of garlic slices. Journal of Food Engineering, 29(1), 75–97.
[15] Matheswaran, M. M., Arjunan, T. V., & Senthilkumar, D. (2018). Analytical exergy evaluation of single pass jet impingement solar air heater. Journal of Thermal Analysis and Calorimetry, 132(1), 583–596.
[16] Mohanraj, M., & Chandrasekar, P. (2009). Performance of a forced convection solar dryer integrated with gravel as sensible heat storage material. Solar Energy, 83(7), 1128–1133.
[17] Shanmugam, V., & Natarajan, E. (2006). Experimental investigation of an indirect solar dryer integrated with desiccant bed. Renewable Energy, 31(7), 1017–1028.
[18] Tiwari, S., & Tiwari, G. N. (2016). Energy, exergy, environmental and economic analysis of an active solar distillation system. Desalination, 398, 121–129.
[19] Usub, T., Lertsatitthanakorn, C., & Wiset, L. (2010). Experimental performance and economic evaluation of an indirect solar tunnel dryer. Applied Energy, 87(1), 127–133.
[20] Yaldiz, O., Ertekin, C., & Uzun, H. I. (2001). Mathematical modeling of thin layer solar drying of green pepper. Energy, 26(5), 457–465.

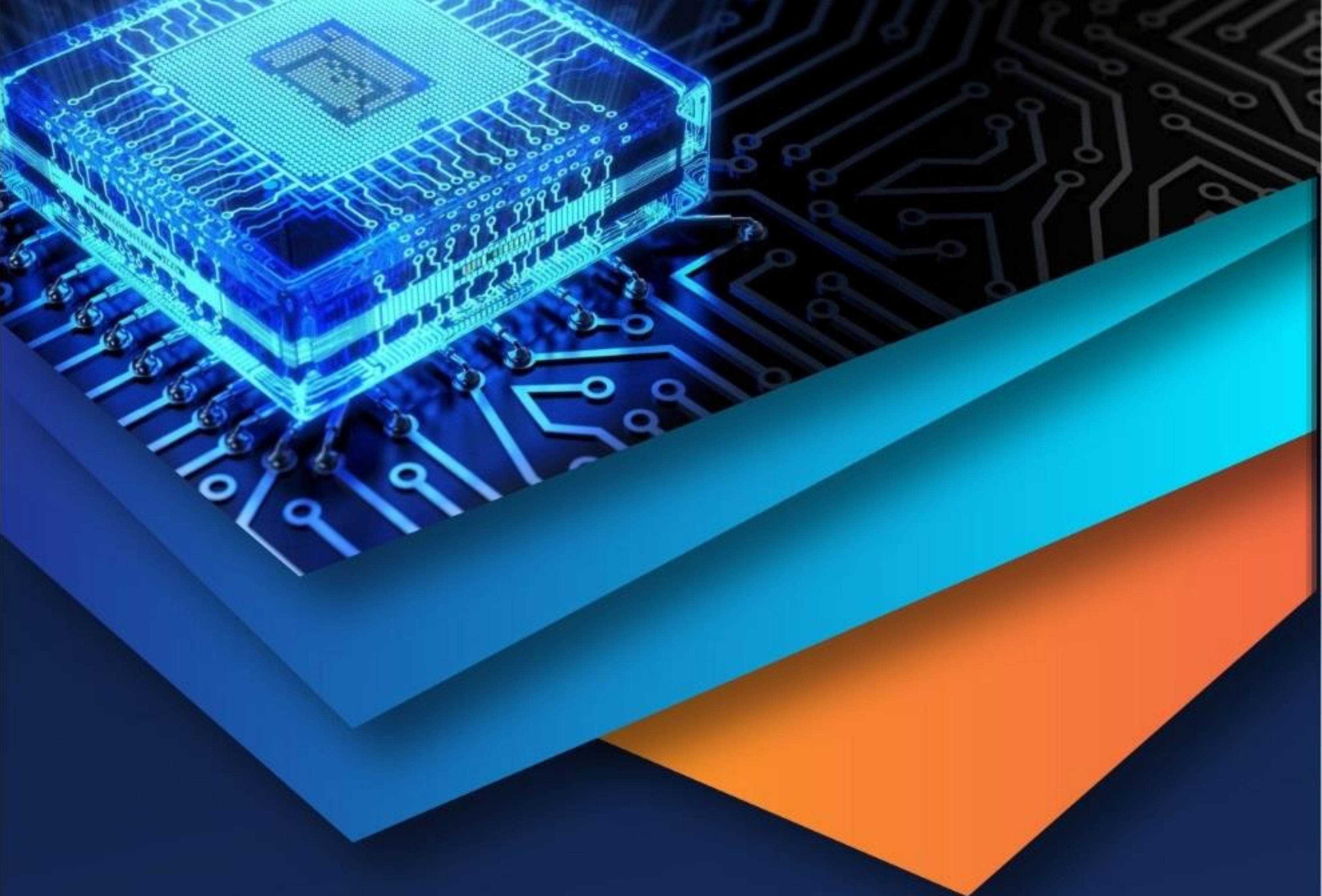

10.22214/IJRASET

INDEX COPERNICUS
45.98

IMPACT FACTOR:
7.129

TOGETHER WE REACH THE GOAL

IMPACT FACTOR:
7.429

INTERNATIONAL JOURNAL FOR RESEARCH

IN APPLIED SCIENCE & ENGINEERING TECHNOLOGY